Effects of Ni doping on the structural properties and collapse of magnetic ordering in $NdFe_{1-x}Ni_xO_3$ ($0.1 \leq x \leq 0.7$) orthoferrites

I. Ahmad[1,2], M. J. Akhtar[2,†], and M. Siddique[2]

[1] *Department of Metallurgy and Materials Engineering, PIEAS, Islamabad, Pakistan*
[2] *Physics Division, PINSTECH, P. O. Nilore, Islamabad, Pakistan*

(Received 11 August 2015; revised manuscript received 23 September 2015; published online 10 January 2016)

$NdFe_{1-x}Ni_xO_3$ ($0.1 \leq x \leq 0.7$) orthoferrites are synthesized by solid state reaction method, and the structural properties of these materials are investigated by employing x-ray diffraction (XRD), scanning electron microscopy (SEM) and Mössbauer spectroscopy. The orthorhombic structure is observed in all systems; however, with the increase in Ni doping, the increase in tolerance factor and the decrease in the cell volume are observed. Orthorhombic distortion decreases with Ni content increasing up to 50%, while above 50% Ni doping it increases. SEM examination indicates the increases in grain size and intermixing of grains with increase in Ni concentration. Comparison between bulk and theoretical densities shows that in each of all samples porosity is less than 2%. Mössbauer spectroscopic investigations are performed to explain local structure, Fe oxidation states and collapse of the magnetic ordering. In these samples the Fe oxidation state remains +3 and there is no considerable increase in hole states observed; however due to mismatch of the ionic radii between Fe^{3+} and Ni^{3+}, octahedral distortions, sagging and distribution of hyperfine parameters increase with increase in Ni concentration. The major factors behind the collapse of magnetic ordering in the Ni-doped systems are the weakening of the super-exchange interactions, decrease in the Neel temperature, increase in spin–spin relaxation frequency and high spin to low spin transition.

Keywords: ceramic, crystal structure, electron microscopy, Mössbauer spectroscopy

PACS: 81.05.Je, 61.50.−f, 68.37.Hk, 33.45.+x **DOI:** 10.1088/1674-1056/25/2/028101

1. Introduction

The perovskite-based ceramic oxides are well known due to their excellent oxidation resistances, chemical stabilities, structural, electrical, magnetic, and mechanical properties. Owing to these properties oxide-based ceramics are widely used in numerous areas.[1–3] $RFe_{1-x}B_xO_3$ orthoferrites (where R denotes a rare earth ion and B a transition metal ion such as Ni, Co, Mn, Cr) are one of the most studied classes of perovskites. Doping at B-sites affects the physical properties with change in their ionic radii, oxidation states and spin states which play a key role in determining the structural, electronic and magnetic properties.[3–6]

The structure of $NdFeO_3$ is orthorombically distorted derivative of cubic perovskites with *Pbnm* symmetry. The crystallographic unit cell of $NdFe_{1-x}Ni_xFeO_3$ can be visualized as three-dimensional (3D) tilted, slightly deformed and corner sharing FeO_6 octahedron while the A-site cations (Nd^{3+}) are dodecahedrally coordinated by 12 O^{2-} ions and fit in the cavities comprised of eight FeO_6/NiO_6 octahedra. The Neel temperature of $NdFeO_3$ is 760 K which decreases with the increase in nickel content. Each Fe ion is coupled by superexchange interaction with six nearest Fe ions, resulting in antiferromagnetic ordering while weak ferromagnetism is observed due to canting of spins.[5–9]

Strong interactions among localized moments, magnetic ordering, itinerant electrons, and spin canting, normally result in the interesting phenomenon in these materials. Owing to these factors, the ABO_3 type perovskite materials exhibit huge variations in properties; which are observed due to the changes in oxidation and spin states, local structural, and chemical factors, difference in band gap, octahedral tilting, cations displacements, colossal polarizeability (with electronic, ionic, and dipolar polarization mechanisms) and relaxer like properties. These perovskites are widely studied both theoretically and experimentally due to very broad range of electrical properties from insulators to superconductors, metal to insulator transitions, magnetic properties, magneto-resistive properties, electrochemical and catalytic properties. Owing to these properties transition metal oxides have become important materials for several high-tech applications such as solid oxide fuels cells, gas sensors, catalysis, spin valves, magnetic field sensors, magnetic sensors, electro-magnets, spintronic devices, oxygen permeable membranes, environmental monitoring applications, random access memory devices based on capacitive components, miniaturization of device sizes, multilayer ceramic capacitors, dielectric substrates, thermoelectric power conversion microwave components for communication systems, etc.[10–20]

When Ni is doped at the Fe sites in orthoferrites, a transition from insulating to metallic state is observed. The difference in ionic radius between Fe^{3+} and Ni^{3+} produces structural distortions. According to the rigid band model, the Fe^{3+} ions have more localized states as compared with the Ni^{3+}

†Corresponding author. E-mail: javedakhtar6@gmail.com

© 2016 Chinese Physical Society and IOP Publishing Ltd

ions, thus the nickel doping in orthoferrites increases the concentration and delocalization of charge carriers.[5,21,22] The RNiO$_3$-type nickelates are paramagnetic metallic oxides due to the presence of Ni^{3+} in low spin state with its e_g electrons having no localized moments. The t_{2g} band of these systems is completely filled and conduction band is created by the hybridization of the Ni^{3+} e_g orbitals and O^{2-} 2p orbitals.[23] In NdFeO$_3$ the Fe ions are in high spin state. The Ni doping in this system can increase oxidation state of the iron ions only if the nickel ions are present in mixed oxidation states (+2 and +3) and oxygen stoichiometry of the system is also maintained which may result in an increase in hole state. Idrees *et al.* have observed increase in hole states and presence of Fe^{4+} with the increase in Ni concentration in LaFe$_{1-x}$Ni$_x$O$_3$.[24,25] Makhdoomi *et al.*[26] have reported the transition of Fe^{3+} ions from high spin to low spin in PrFe$_{1-x}$Ni$_x$O$_3$ orthoferrite system with the increase in Ni concentration. Fe, Co and Ni are neighbors in the periodic table and NdFeO$_3$, NdCoO$_3$, and NdNiO$_3$ crystallize in the same crystal structure; however, NdFeO$_3$ is an insulator, NdCoO$_3$ is a semiconductor and NdNiO$_3$ shows a metallic behavior.[7] The metallic or insulating behaviors of these materials dependon the extent of distortion from ideal cubic perovskite structure and on B–O–B bond angle.[5] Rao *et al.*[27] studied the LaNi$_{1-x}$Fe$_x$O$_3$ system and found that the itinerancy raises with the increase in the nickel concentration. They also observed that the increase in covalent character of B–O bond results in itinerant behavior of perovskite oxide, with B-site cation in the low spin state. Furthermore, the charge carriers of ABO_3 oxide having higher ionic character of B–O bond will be localized and in this case the B-site cations will be in the high spin state.

In NdFe$_{1-x}$Ni$_x$O$_3$ system both Fe and Ni are magnetic 3d transitions metals, and show magnetic ordering below T_N which is $\sim$ 700 K for NdFeO$_3$ and $\sim$ 200 K for NdNiO$_3$. The exchange interaction between B-site ion and Nd ions can be divided into isotropic and anisotropic components. The isotropic exchange is canceled by compensating for contributions from anti-parallel moments. However, the anisotropic exchange is not completely compensated for, which results in the appearance of internal field $H_{Nd–B}$ and polarizes the Nd sub-lattice at lower temperatures both in NdFeO$_3$ and NdNiO$_3$. Magnetic vacancies are introduced into the Fe sub-lattices when iron ions are substituted by non-magnetic ions. This results in the dilution of the Fe sub-lattices which stimulates the lowering of Neel temperature till quenching of magnetic ordering.[28]

Tin oxide and zinc oxide are widely studied materials as gas sensors but these materials have poor stabilities and selectivities which restricted their usefulness as gas sensing materials. Doped and undoped perovskite oxides are other types of materials which are extensively studied as gas sensors due to superior selectivity. Zhang *et al.*[29] have studied the CO gas sensing properties of NdFe$_{1-x}$Co$_x$O$_3$ system and observed that NdFeO$_3$ has very good response as CO gas sensor.

In this work NdFe$_{1-x}$Ni$_x$O$_3$ orthoferrites are synthesized by solid state reaction method and characterized by XRD, pycnometer, SEM and Mössbauer spectroscopy.

2. Experiment

Polycrystalline NdFe$_{1-x}$Ni$_x$O$_3$, (where $x = 0.1$, 0.2, 0.3, 0.4, 0.5, 0.6, and 0.7), samples were synthesized in air by a conventional solid state reaction method, using high purity (99.99%) Nd_2O_3, NiO and Fe_2O_3 obtained from Sigma Aldrich. To obtain a homogenous mixture, stoichiometric quantities of all the chemicals were mixed in highpurity acetone followed by grinding. Appropriate measures were taken to ensure that starting materials are moisture free, by preheating at 100 °C for 2 h before weighing. The mixtures of oxides were heated at 1000 °C, 1100 °C, and 1200 °C for 16 h at each temperature with intermediate grinding. After this heat treatment, circular pellets of 10-mm diameter and $\sim$ 1.5-mm thicknesses were fabricated from the ground powder under a pressure of 3 tons/inch^2 (1 ton = 1.01605 t, 1 inch = 2.54 cm). These pellets were finally sintered at 1300 °C for 16 h. Heating rate was maintained at 5 °C/min during sintering at each temperature, while all samples were cooled in closed off furnace. The phase purity of each sintered pellet was confirmed by x-ray diffraction (XRD) using Cu K_α radiation (1.5418 Å). The room temperature XRD data were collected for $20^\circ \leq 2\theta \leq 70^\circ$ with 0.02° scanning step size and 3 s per step counting time. In order to calculate the lattice parameters, least square fitting technique was used. Densities of these sintered pallets were measured using pycnometer. SEM analyses of all these samples were performed using SEM LEO 440i. For SEM analysis each sintered pallet was fractured perpendicularly to the circular plane and analyses of these fractured samples were carried out. Fe^{57} Mössbauer spectra were taken at room temperature in transmission mode using the Co^{57} in Rh matrix as a source of γ-rays. For the calibration of Mössbauer spectrometer, a thin α-Fe foil was used. MOS-90 computer program was used to analyze the Mössbauer data; where analysis was performed on the assumption that all peaks are Lorentzian in shape.

3. Results and discussion

Figure 1 shows the XRD patterns of freshly synthesized samples of NdFe$_{1-x}$Ni$_x$O$_3$, (where $x = 0.1$–0.7), collected at room temperature. All peaks are successfully indexed on the basis of PCPDF card Nos. 82-2421, 82-2422, 82-2158, and 81-2245.[5,6,30] The XRD results show that single phase orthorhombic perovskite structure having space group *Pbnm* has been synthesized. However in 50% Ni-doped sample two very small peaks due to a minor tertragonal $Nd_4Ni_3O_8$ phase are observed. The lattice parameters, a, b, and c, calculated from XRD data are shown in Table 1 which are consistent with those

earlier reported.[4,5,31,32] With the increase in the nickel concentration, XRD peaks shift towards higher 2θ indicating that the cell volume decreases as the Ni concentration is increased. This decrease in unit cell volume might be due to the difference in ionic radius between Ni^{3+} (0.60 Å) and Fe^{3+} (0.645 Å) in high spin states.[33]

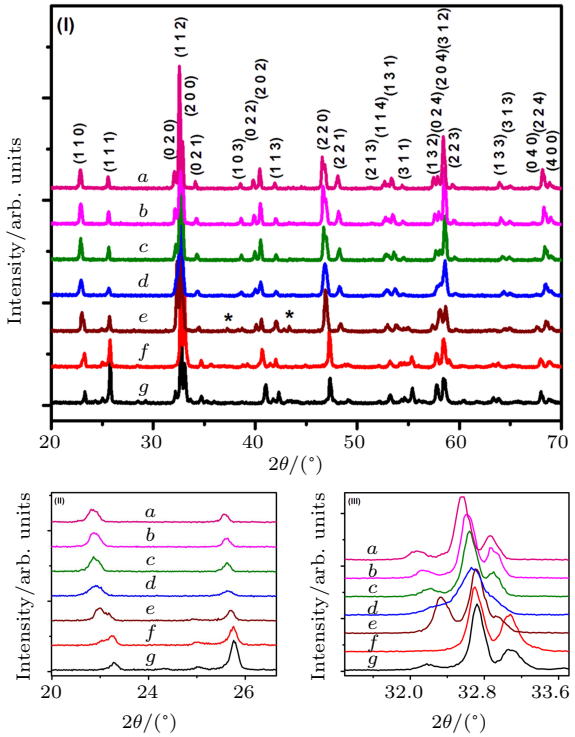


Fig. 1. (color online) XRD patterns of (curve *a*) $NdFe_{0.9}Ni_{0.1}O_3$, (curve *b*) $NdFe_{0.8}Ni_{0.2}O_3$, (curve *c*) $NdFe_{0.7}Ni_{0.3}O_3$, (curve *d*) $NdFe_{0.6}Ni_{0.4}O_3$, (curve *e*) $NdFe_{0.5}Ni_{0.5}O_3$, (curve *f*) $NdFe_{0.4}Ni_{0.6}O_3$, and (curve *g*) $NdFe_{0.3}Ni_{0.7}O_3$ collected at room temperature. Symbol $*$ indicates peaks due to a minor tetragonal $Nd_4Ni_3O_8$ phase.

In Table 2, the values of Goldsmith tolerance factor are given, which show an increasing trend with the increase in nickel concentration. Goldsmith tolerance factor (t) has been calculated by using the following relation:

$$t = \frac{d_{\mathrm{A-O}}}{\sqrt{2}\,(d_{\mathrm{B-O}})} = \frac{r_{\mathrm{A}} + r_{\mathrm{O}}}{\sqrt{2}(r_{\mathrm{B}} + r_{\mathrm{O}})}. \tag{1}$$

For the calculation of tolerance factors the ionic sizes are cited from Ref. [33] by Shannon. It is evident from these results that the values of Goldsmith tolerance factor (t) increase slightly with the increase in Ni.

The orthorhombic distortion parameter (D), which is a measure of deviation of unit cell from ideal cubic structure and is represented by the following formula:[34]

$$D = \frac{1}{3}\sum_{i=1}^{3}\left|\frac{\alpha_i - \bar{\alpha}}{\bar{\alpha}}\right| \times 100. \tag{2}$$

In this formula, $\alpha_1 = a$, $\alpha_2 = b$, $\alpha_3 = c/\sqrt{2}$, and

$$\bar{\alpha} = (abc/\sqrt{2})^{1/3}.$$

From Table 2, we observe that the values of orthorhombic distortion decrease with nickel concentration increasing up to 50% and with further increase in Ni contents the orthorhombic distortion increases again. This may be due to the fact that when Ni concentration is 50% the numbers of Fe and Ni atoms become equal which may produce symmetry in structure and minimum value of orthorhombic distortion is observed. However, the further increase in concentration of Ni, the numbers of Fe and Ni atoms again become different, causing an increase in the value of D.

Table 1. Phase symmetry, cell parameters a, b, and c, and cell volumes of $NdFe_{1-x}Ni_xO_3$.

Sample	Phase symmetry	a/Å	b/Å	c/Å	Cell volume/Å^3
$NdFe_{0.9}Ni_{0.1}O_3$	orthorhombic	5.4540	5.5805	7.7649	236.333
$NdFe_{0.8}Ni_{0.2}O_3$	orthorhombic	5.4448	5.5708	7.7524	235.145
$NdFe_{0.7}Ni_{0.3}O_3$	orthorhombic	5.4433	5.5629	7.7359	234.247
$NdFe_{0.6}Ni_{0.4}O_3$	orthorhombic	5.4404	5.5447	7.7351	233.332
$NdFe_{0.5}Ni_{0.5}O_3$	orthorhombic	5.4400	5.5381	7.7219	232.640
$NdFe_{0.4}Ni_{0.6}O_3$	orthorhombic	5.4396	5.5412	7.7083	232.343
$NdFe_{0.3}Ni_{0.7}O_3$	orthorhombic	5.4393	5.5368	7.6717	231.043

Table 2. Calculations of Goldsmith tolerance factor, orthorhombic distortion parameter, XRD density, bulk density, and calculated porosity of $NdFe_{1-x}Ni_xO_3$ samples.

Sample	Goldsmith tolerance factor (t)	Orthorhombic distortion parameter (D)	XRD density d_{th}/g·cm^{-3}	Bulk density d/g·cm^{-3}	Calculated porosity P/%
$NdFe_{0.9}Ni_{0.1}O_3$	0.92525	0.8714	6.97946	6.84098	1.9841
$NdFe_{0.8}Ni_{0.2}O_3$	0.92729	0.8673	7.02288	6.91294	1.5654
$NdFe_{0.7}Ni_{0.3}O_3$	0.92935	0.8579	7.05776	6.95674	1.4313
$NdFe_{0.6}Ni_{0.4}O_3$	0.93141	0.7260	7.09355	7.00733	1.2154
$NdFe_{0.5}Ni_{0.5}O_3$	0.93348	0.7127	7.12278	7.03495	1.2331
$NdFe_{0.4}Ni_{0.6}O_3$	0.93557	0.7787	7.14003	7.04467	1.3356
$NdFe_{0.3}Ni_{0.7}O_3$	0.93766	0.8601	7.18839	7.07634	1.5587

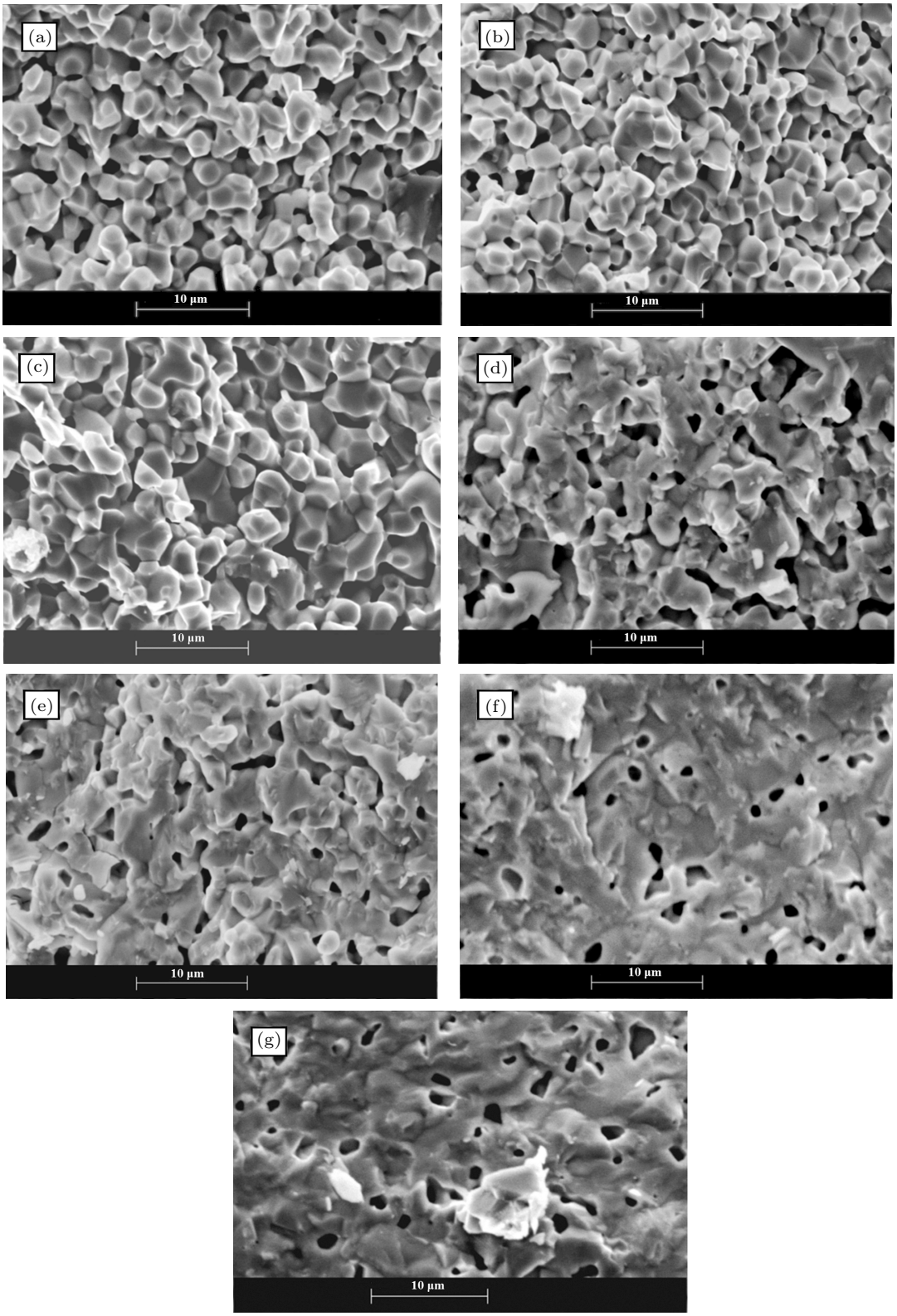


Fig. 2. SEM micrographs (at 3000× magnification) taken from the fractured surfaces of the sintered pellets of (a) $NdFe_{0.9}Ni_{0.1}O_3$, (b) $NdFe_{0.8}Ni_{0.2}O_3$, (c) $NdFe_{0.7}Ni_{0.3}O_3$, (d) $NdFe_{0.6}Ni_{0.4}O_3$, (e) $NdFe_{0.5}Ni_{0.5}O_3$, (f) $NdFe_{0.4}Ni_{0.6}O_3$, and (g) $NdFe_{0.3}Ni_{0.7}O_3$.

The density of the material is an important parameter; the bulk density must be above ninety percent of the theoretical density for the determination of electrical and thermal properties.[35] The bulk density of each of $NdFe_{1-x}Ni_xO_3$ samples is measured using pycnometer while the theoretical density is calculated from the following equation:

$$d_{\text{th}} = ZM/NV \text{ (in units g/cm}^3\text{)}, \tag{3}$$

where Z is the number of formula units in one unit cell and

its value is 4 for $GdFeO_3$-type structures, M is atomic mass in gram, here the deviation from any stoichiometry is not taken into account in calculating M, N is Avogadro's number, and V is volume in unit cm^3. Porosity of each sample is calculated from the values of theoretical density (d_{th}) and bulk density (d). Porosity (P) in percentage is calculated for each sample using the following relation:

$$P = (1 - d/d_{th}) \times 100. \quad (4)$$

The results of theoretical density (d_{th}), bulk density (d) and calculated porosity (P) are also shown in Table 2. From these results it is observed that in all samples porosity values are less than 2 percent and bulk density is above 98 percent as compared with the theoretical density which is advantageous for measuring the electrical and thermal properties.

In order to investigate the effects of nickel doping on the particle size, porosity, grain connectivity and grain boundary, we have carried out scanning electron microscopy (SEM). The SEM micrographs of the $NdFe_{1-x}Ni_xO_3$ pellets (fractured face) sintered at 1300 °C are shown in Figs. 2(a)–2(g) at 3000× magnification. The SEM analyses are performed at room temperature; from these micrographs the grain connectivities, grain boundary areas, grain sizes, and grain shapes are clearly visible. The lower doping samples have more regular grain shapes and with the increase in Ni content the grain connectivity and grain size gradually increase. The SEM results infer that grains intermixing increase with the increase in Ni concentration. Some grains, especially in lower doping samples, have well defined geometrical shapes and sharp grain boundaries; with the increase in nickel content there is a gradual reduction in grain boundary area. The observed pore size varies from area to area and sample to sample but mostly their sizes are all less than 1 μm. The pores are produced mainly due to the effect of sintering temperature, applied pressure and pressing time for making palates while the disorientation and mismatch of grains and grain boundaries can also play an important role.

The effects of Ni doping on the local environment of Fe sites in $NdFe_{1-x}Ni_xO_3$ ($0.1 \leq x \leq 0.7$) are investigated by Mössbauer spectroscopy to explore the roles of Ni doping in the oxidation state of Fe, octahedral distortions and the change in the strength of magnetic ordering. The Mössbauer spectra of $NdFe_{1-x}Ni_xO_3$ ($0.1 \leq x \leq 0.7$) samples are shown in Fig. 3 and their fitted parameters are summarized in Table 3. The Mössbauer spectrum for 10% Ni is very well fitted with a magnetic sextet and a small paramagnetic singlet [Fig. 3(a)]. In an earlier study we have reported the Mössbauer spectrum of $NdFeO_3$ in which only a magnetic sextet was observed.[35,36] This indicates that the appearance of a small singlet is due to paramagnetic phase formed due to Ni doping. The internal magnetic, H_{eff} also decreases with Ni doping indicating the paramagnetic behavior of Ni in this system. From the isomer shift values it is inferred that oxidation state of iron is Fe^{3+} in the whole system. The quadrupole splitting is very sensitive parameter to probe the local environment of Fe and its value close to zero represents no distortion in Fe octahedron in this system. The line broadening can be related to the hyperfine field distribution originating from the non-equivalent Fe sites in the crystal symmetry.

The Mösbasuer spectra of $NdFe_{1-x}Ni_xO_3$ ($0.2 \leq x \leq 0.5$) are shown in Figs. 3(b)–3(e) and the fitted parameters of these samples are given in Table 3. In these samples the local distortions and strains caused by the A-site cations keep almost similar and changes are mainly observed due to B-site cations. The spectra of these four samples are fitted by two sextets and one singlet. The appearance of more than one sextet is ascribed to dissimilar distributions of nickel ions around iron ions. The decrease in internal magnetic field (H_{eff}) clearly shows that the

Table 3. Values of magnetic hyperfine field (H_B), isomer shift (IS), quadrupole splitting (Δ), line width (Γ), and relative area (%) associated with each spectral feature in ^{57}Fe Mössbauer spectra of $NdFe_{1-x}Ni_xO_3$. The unit 1 Oe = 79.5775 $A{\cdot}m^{-1}$.

Sample		H_{eff}/kOe	IS/$mm{\cdot}s^{-1}$	Δ/$mm{\cdot}s^{-1}$	Γ/$mm{\cdot}s^{-1}$	Relative area/%
$NdFe_{0.9}Ni_{0.1}O_3$	sextet *A*	513	0.38	−0.010	0.44	99
	singlet	—	0.41	—	1.17	1
$NdFe_{0.8}Ni_{0.2}O_3$	sextet *A*	495	0.39	−0.026	0.41	30
	sextet *B*	470	0.37	−0.027	0.80	68
	singlet	—	0.34	—	0.65	2
$NdFe_{0.7}Ni_{0.3}O_3$	sextet *A*	441	0.36	−0.041	0.66	34
	sextet *B*	399	0.36	−0.036	1.34	63
	singlet	—	0.29	—	0.68	3
$NdFe_{0.6}Ni_{0.4}O_3$	sextet *A*	414	0.36	−0.058	0.86	37
	sextet *B*	362	0.28	−0.151	1.61	47
	singlet	—	0.32	—	0.89	16
$NdFe_{0.5}Ni_{0.5}O_3$	sextet *A*	411	0.35	0.041	1.82	16
	sextet *B*	355	0.35	−0.019	5.88	77
	singlet	—	0.30	—	1.32	7
$NdFe_{0.6}Ni_{0.4}O_3$	singlet	—	0.36	—	1.07	100
$NdFe_{0.7}Ni_{0.3}O_3$	singlet	—	0.37	—	0.99	100

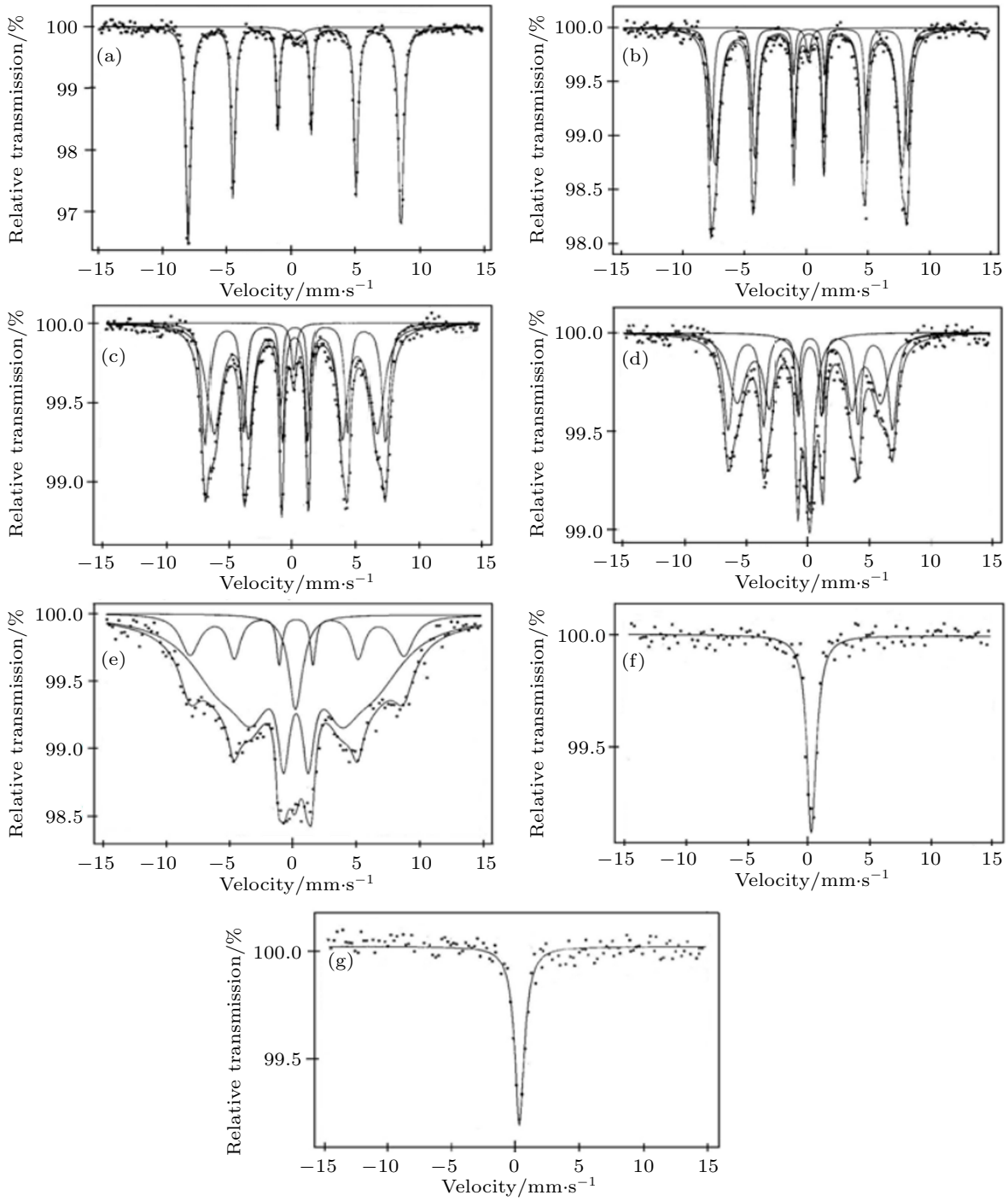


Fig. 3. The room temperature Mössbauer spectra of (a) $NdFe_{0.9}Ni_{0.1}O_3$, (b) $NdFe_{0.8}Ni_{0.2}O_3$, (c) $NdFe_{0.7}Ni_{0.3}O_3$, (d) $NdFe_{0.6}Ni_{0.4}O_3$, (e) $NdFe_{0.5}Ni_{0.5}O_3$, (f) $NdFe_{0.4}Ni_{0.6}O_3$, and (g) $NdFe_{0.3}Ni_{0.7}O_3$.

magnetic ordering decreases with the increase in nickel concentration. The quadrupole splitting values increase gradually with Ni content increasing up to 40% indicating that there is an increase in the concentration of Fe ions which are slightly shifted from their octahedral sites. Thus the octahedral distortions in the local structure increase up to 40%. However, for 50% Ni doped sample a decrease in quadrupole splitting is observed which may be because more symmetric arrangements, owing to the equal number of Fe and Ni atoms at *B*-sites, form BO_6 octahedra. With the increase in Ni concentration the line width also increases, indicating an increase in sagging and distribution of hyperfine parameters. The line broadening observed in these samples indicates the gradual collapse of magnetically ordered state into spin disordered state. The decrease in average internal magnetic field with the increase of Ni-concentration, as deduced from the Mössbauer results, can be seen in Fig. 4.

The Mösbasuer spectra of $NdFe_{1-x}Ni_xO_3$ ($0.6 \leq x \leq 0.7$) are shown in Figs. 3(f) and 3(g) and the fitted parameters of these samples are also given in Table 3. The Mössbauer spectra of both samples are fitted with a singlet only indicating that magnetic ordering is completely lost from the samples doped

with 60% and higher Ni.

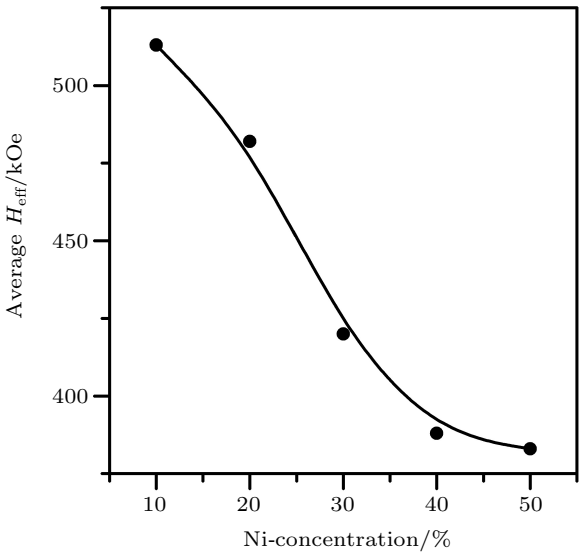


Fig. 4. Variation of average internal magnetic field with Ni concentration in $NdF_{1-x}Ni_xO_3$.

As observed by the Mössbauer spectra and broadening or sagging of the magnetically split lines, a progressive collapse of magnetic ordering is observed with the increase in Ni concentration of $NdFe_{1-x}Ni_xO_3$ ($0.1 \leq x \leq 0.7$). It is interesting to note that the collapse of magnetic ordering is also observed in other Ni-doped $LaFeO_3$, $PrFeO_3$, and $NdFeO_3$ orthoferrite systems.[4,37–39]

Makhdoomi *et al.*[38] observed that in $PrFe_{1-x}Ni_xO_3$ system when octahedral distortions around Fe^{3+} increase, it results in the increase in crystal field splitting energy which becomes higher than average spin pairing energy of electrons. Consequently, due to the spin crossover the high spin configuration of Fe^{3+} (with 5 unpaired spins) is converted into low spin (with only one unpaired spin) one. But the observed magnetic field values for up to 50% Ni samples are higher than the expected field due to low spin of Fe^{3+} with 5 t_{2g} and zero e_g electrons in the valence shell. Thus up to 50% Ni concentration samples, Fe is not converted into low spin configuration while in higher doped samples it may be the case.

In the case of $LaFe_{1-x}Ni_xO_3$ system, Marzec[39] explained the transition from a magnetically ordered state to a spin disordered state by a spin–spin relaxation phenomenon which becomes faster than the characteristic Mössbauer experiment time window with Ni doping. The increase in spin–spin relaxation frequency with temperature can account for the temperature-dependent sagging of the sextet and collapse of the magnetically order state above Neel temperature into orthoferrites.[37–40] With the increase in nickel concentration, a progressive increase in itinerant behavior is observed and results in less localized electron spins. Consequently, the spin relaxation becomes easier which results in the progressive collapse of the magnetically ordered state into spin disordered state. Asai and Sekizawa[41] also established that in these materials progressive sagging of sextet increases with the decrease in characteristic relaxation time constant.

The strength of the super-exchange interaction in orthoferrites depends upon the nature of *B*-site cation and the *B*–O–*B* bond angle. Thus the collapse of magnetic ordering, sagging behavior and decrease in Neel temperature can also be correlated with the weakening of super-exchange interactions. As a result of doping, the Fe^{3+}–O^{2-}–Fe^{3+} interactions in $NdFeO_3$ become Fe^{3+}–O^{2-}–Fe^{3+}, Fe^{3+}–O^{2-}–Ni^{3+}, and Ni^{3+}–O^{2-}–Ni^{3+} interactions in $NdFe_{1-x}Ni_xO_3$ ($0.1 \leq x \leq 0.7$). The super-exchange angle also changes which leads to a decrease in super-exchange interactions with the increase in Ni content. It is inferred that all above factors contribute to the collapse of magnetic ordering with the increase of Ni concentration in $NdFe_{1-x}Ni_xO_3$.

4. Conclusions

In the present study polycrystalline $NdFe_{1-x}Ni_xO_3$ ($0.1 \leq x \leq 0.7$) orthoferrites are synthesized by a solid state reaction method. From the XRD results it is found that the orthorhombic structure is retained in each of all samples; however, by increasing the Ni concentration, tolerance factor increases while cell volume decreases. The orthorhombic distortion is found to decrease with Ni concentration increasing up to 50%, while above 50% Ni doping it starts to increase. The calculated porosity value in these systems are all below 2%. From SEM results it is found that when the concentration of nickel is low, the grains have more regular shapes and with the increase in Ni concentration grain connectivity grain size gradually increases. From these results it is also inferred that the intermixing grains increase with the increase in Ni concentration. The pores size differs from area to area and sample to sample but mostly their sizes are all less than 1 μm. Mössbauer spectroscopic results indicate that the oxidation state Fe ion is Fe^{+3} for each of all samples. The increase in distribution of hyperfine parameters and the decrease in magnetic ordering with the increase in nickel concentration are also observed. The major factors behind the collapse of magnetic ordering in this orthoferrite system may be the weakening of superexchange interactions, the transition from high spin to low spin and the increase in spin–spin relaxation frequency due to the increase in the delocalization of charge carriers.

Acknowledgment

One of the authors, Irfan Ahmad thanks the Higher Education Commission (HEC) of Pakistan for the financial support through 5000 Indigenous Scholarship Scheme in Physical Sciences Batch-V for his Ph. D studies. The authors are grateful to Dr. Shahid Khan Durrani, MD, PINSTECH and Dr. M. Iqbal, PD, PINSTECH for providing XRD and SEM facilities, respectively and also thank PAEC for supporting this project.

References

[1] Minh N Q 1993 *J. Am. Ceram. Soc.* **76** 563
[2] Tokura Y 2003 *Physics Today* **56** 50
[3] Hou X, Ji D H, Qi W H, Tang G D and Li Z Z 2015 *Chin. Phys. B* **24** 057501
[4] Bashir A, Ikram M, Kumar R, Thakur P, Chae K, Choi W and Reddy V 2009 *J. Phys.: Conden. Matter* **21** 325501
[5] Blasco J and García J 1994 *J. Phys. Chem. Solids* **55** 843
[6] Blasco J and García J 1994 *Solid State Commun.* **91** 381
[7] Tiwari A and Rajeev K P 1998 *Solid State Commun.* **109** 119
[8] Ahmad I, Akhtar M J and Hasan M M 2014 *Mater. Res. Bull.* **60** 474
[9] Ahmad I, Akhtar M J, Khan R T A and Hasan M M 2013 *J. Appl. Phys.* **114** 034103
[10] Zaanen J, Sawatzky G A and Allen J W 1985 *Phys. Rev. Lett.* **55** 418
[11] Park C Y, Azzarello F V and Jacobson A J 2006 *J. Mater. Chem.* **16** 3624
[12] Guo M C, Liu W F, Wu P, Zhang H, Xu X L, Wang S Y and Rao G H 2015 *Chin. Phys. Lett.* **32** 066101
[13] Naumovich E, Patrakeev M, Kharton V, Islam M. Yaremchenko A, Frade J and Marques F 2006 *Solid State Ionics* **177** 457
[14] Choi J J, Lee J H, Park D S, Hahn B D, Yoon W H and Lin H T 2007 *J. Am. Ceram. Soc.* **90** 1926
[15] Didosyan Y, Barash V, Bovarin N, Hauser H and Fulmek P 1997 *Sens. Actuat. A: Phys.* **59** 56
[16] Mathur N, Burnell G, Isaac S, Jackson T, Teo B S, MacManus-Driscoll J, Cohen L, Evetts J and Blamire M 1997 *Nature* **387** 266
[17] Sarma S D 2003 *Nat. Mater.* **2** 292
[18] Carotta M C, Martinelli G, Sadaoka Y, Nunziante P and Traversa E 1998 *Sens. Actuat. B: Chem.* **48** 270
[19] Zhu X, Wang J, Zhang Z, Zhu J, Zhou S, Liu Z and Ming N 2008 *J. Am. Ceram. Soc.* **91** 2683
[20] Kumar Pradeep, Kashyap Subhash C, Sharma Vijay Kumar and Gupta H C 2015 *Chin. Phys. B* **24** 098101
[21] Idrees M, Nadeem M and Hassan M 2010 *J. Phys. D: Appl. Phys.* **43** 155401
[22] Feroz A Mir, Sharma S K and Ravi Kumar 2014 *Chin. Phys. B* **23** 048101
[23] Idrees M, Nadeem M, Mehmood M, Atif M, Chae K H and Hassan M 2011 *J. Phys. D: Appl. Phys.* **44** 105401
[24] Idrees M, Nadeem M and Siddique M 2013 *Curr. Appl. Phys.* **13** 448
[25] Idrees M, Nadeem M, Shah M and Shin T 2011 *J. Phys. D: Appl. Phys.* **44** 455303
[26] Makhdoomi A B, Ikram M and Kumar R 2010 *J. Magn. Magn. Mater.* **322** 2581
[27] Rao C N R, Parkash O M and Ganguly P 1975 *J. Solid State Chem.* **15** 186
[28] Bartolomé F and Bartolomé J 2005 *Solid State Sci.* **7** 700
[29] Zhang R, Hu J, Han Z, Zhao M, Wu Z, Zhang Yand Qin H 2010 *J. Rare Earths* **28** 591
[30] Lacorre P 1992 *J. Solid State Chem.* **97** 495
[31] Tiwari A 1998 *J. Alloys Compd.* **274** 42
[32] Sławiński W, Przeniosło R, Sosnowska I and Suard E 2005 *J. Phys.: Conden. Matter* **17** 4605
[33] Shannon R 1976 *Acta Crystallogr. A* **32** 751
[34] Kostogloudis G C, Vasilakos N and Ftikos C 1997 *J. Eur. Ceram. Soc.* **17** 1513
[35] Ahmad I, Akhtar M J, Younas M, Siddique M and Hasan M M 2012 *J. Appl. Phys.* **112** 074105
[36] Ahmad I, Akhtar M. J, Siddique M, Iqbal M and Hasan M M 2013 *Ceram. Int.* **39** 8901
[37] Norman A, Morris M and Deeney F 1999 *J. Mater. Proc. Tech.* **92** 118
[38] Makhdoomi A B, Ikram M and Kumar R 2010 *J. Magn. Magn. Mater.* **322** 2581
[39] Marzec J 2007 *J. Power Sources* **173** 671
[40] Kharton V V, Kovalevsky A V, Patrakeev M V, Tsipis E V, Viskup A P, Kolotygin V A, Yaremchenko A A, Shaula A L, Kiselev E A and Waerenborgh J C 2008 *Chem. Mater.* **20** 6457
[41] Asai K and Sekizawa H 1980 *J. Phys. Soc. Jpn.* **49** 90